

Figure S1 Screening of *BubR1*^{+/+} and *BubR1*^{H/H} mice for osteoporosis and analysis of *BubR1*^{+/+}, *BubR1*^{H/H} and *BubR1*^{H/H}/*p16*^{Ink4a-/-} mice for abdominal muscle volume and fat disposition. **(a)** Haematoxylin and eosin-stained longitudinal sections of femurs from a 1-year-old wild-type, a 1-year-old *BubR1* hypomorphic and a 35-month-old wild-type mouse. Scale bar = 100 μ m. **(b)** Quantitation of relative width of the cortical wall to total bone width in sections from a. For each genotype, three male mice were used and 40 random measurements were taken. Note the clear reduction

in bone mass and density in the old wild-type animal, while there is no difference between the 1-year-old samples. Asterisks indicates p value of < 0.0001 compared to 12-month-old wild-type using a two-tailed Mann-Whitney test. Error bars are s.d. **(c)** Analysis of abdominal muscle and fat tissue of 5-month-old wild-type, *BubR1*^{H/H}, and *BubR1*^{H/H}/*p16*^{Ink4a-/-} mice by MRI. Representative cross-sectional MRI images are shown. Areas of muscle (M), fat (F), and the spinal cord (S) are indicated. Note the substantial increase in fat and muscle in *BubR1*^{H/H}/*p16*^{Ink4a-/-} mice.

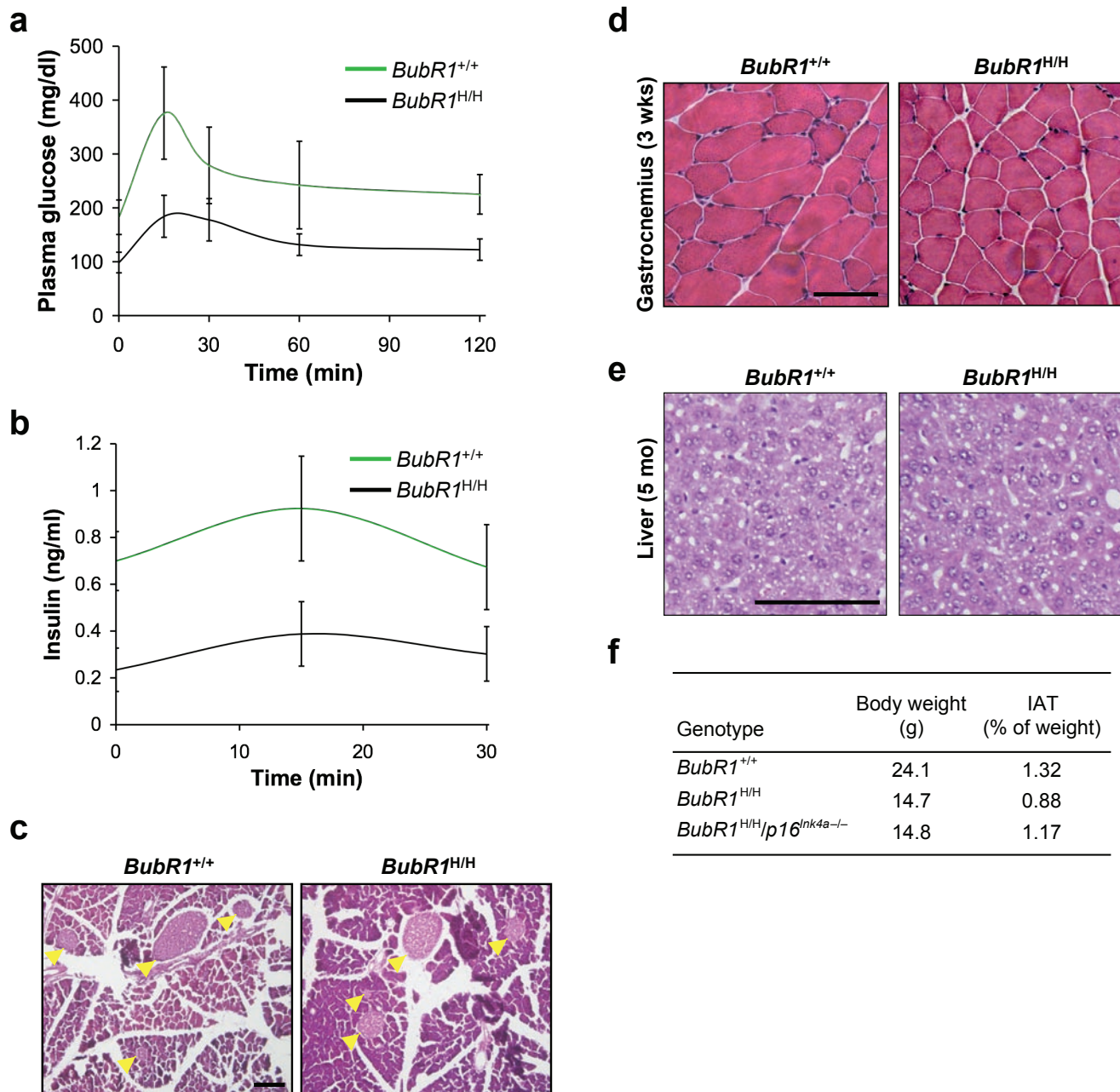


Figure S2 Analysis of pancreatic beta-cell function, young skeletal muscle histology, and fat deposition of *BubR1* hypomorphic mice (**a-c**) *BubR1* hypomorphic mice have normal pancreatic beta-cell function. Changes in blood glucose (**a**) and insulin (**b**) levels after oral glucose administration to 5-month-old *BubR1*^{+/+} and *BubR1*^{H/H} mice ($n = 5$ males for each genotype). Error bars are s.d. (**c**) Hematoxylin and eosin stained pancreas sections of 1-year-old *BubR1*^{+/+} and *BubR1*^{H/H} mice. Arrowheads mark β -cell islets. Scale bar = 100 μ m. (**d**) Muscles of 3-week-old *BubR1*^{H/H} appear normal.

Cross-sections of gastrocnemius muscles from 3-week-old wild-type and *BubR1*^{H/H} mice stained with hematoxylin and eosin. Scale bar = 100 μ m. (**e**) *BubR1* hypomorphic mice do not have fatty livers. Hematoxylin and eosin stained liver sections of 5-month-old *BubR1*^{+/+} and *BubR1*^{H/H} mice. Scale bar = 100 μ m. (**f**) Quantitation of inguinal adipose tissue in 6-week-old *BubR1*^{+/+}, *BubR1*^{H/H} and *BubR1*^{H/H}/*p16*^{Ink4a-/-} mice. IAT is expressed as percentage of total body weight. Three males of each genotype were used. Note that *BubR1*^{H/H} mice lacking *p16*^{Ink4a} have improved fat disposition.

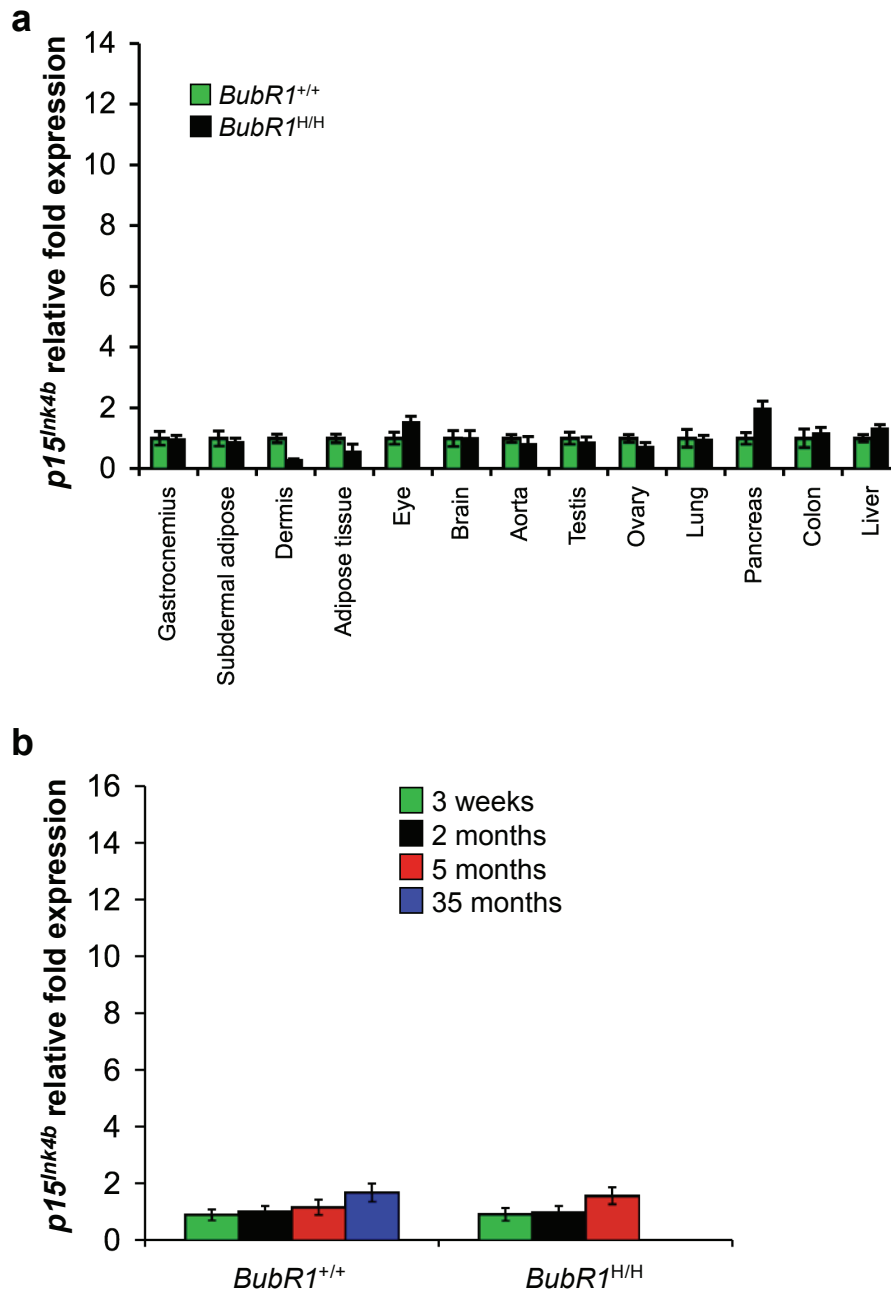


Figure S3 *p15^{Ink4b}* is not induced in response to BubR1 hypomorphism. **(a)** Relative expression of *p15^{Ink4b}* in different tissues of 2-month-old *BubR1*^{H/H} and *BubR1*^{+/+} mice as determined by qRT-PCR (n = 3 males for each genotype). All values were normalized to *GAPDH*. Relative expression is to wild-type samples. Error bars are s.d.

(b) Relative expression of *p15^{Ink4b}* in gastrocnemius muscles of wild-type and *BubR1*^{H/H} males at various ages as measured by qRT-PCR (n = three muscles per genotype and age group). Values were normalized to *GAPDH*. Relative fold expression is to 2-month-old wild-type values. Error bars are s.d.

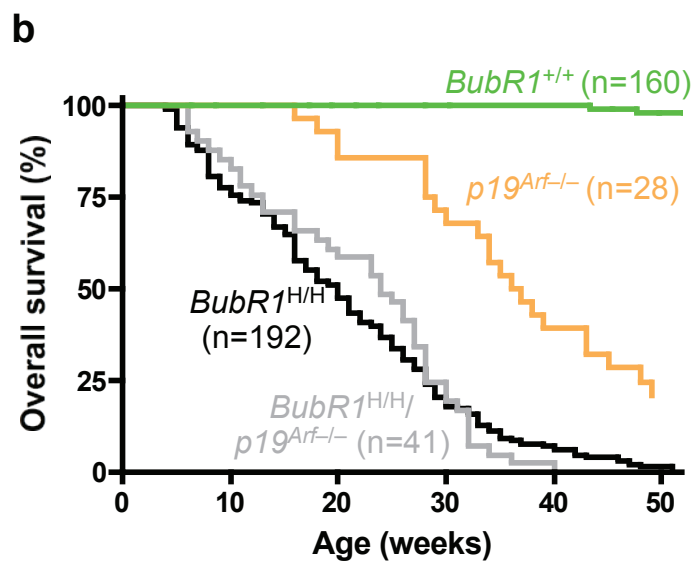
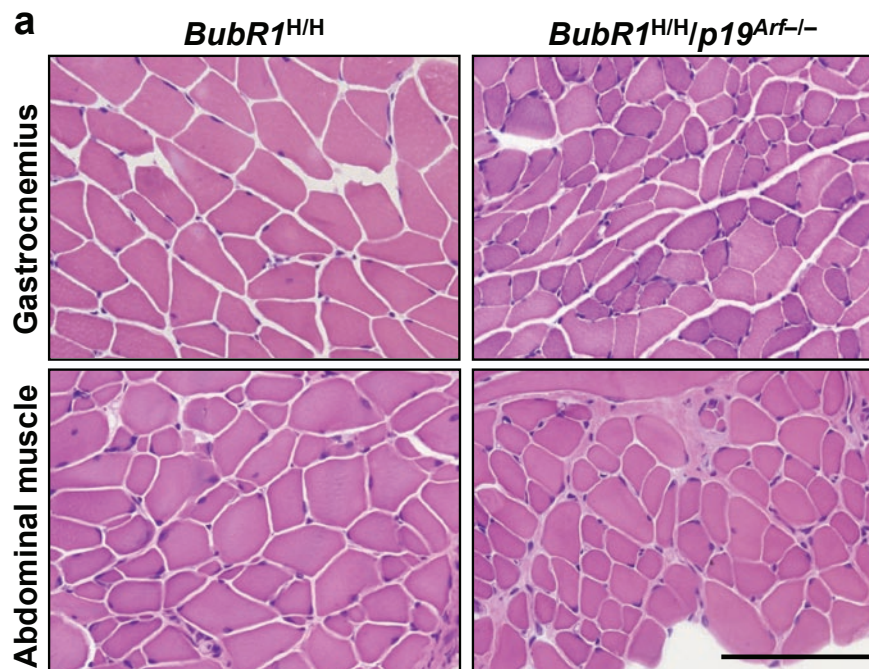


Figure S4 Ablation of p19^{Arf} in BubR1 hypomorphic mice increases muscle wasting but has no impact on lifespan. (a) Cross sections of gastrocnemius and abdominal muscles from 6-week-old *BubR1^{H/H}* and *BubR1^{H/H}/p19^{Arf}^{-/-}* mice. Sections were stained with hematoxylin and eosin. Note that fibers

diameters are typically smaller when p19^{Arf} is lacking. Scale bar = 100 μm. (b) Overall survival curves for wild-type, *p19^{Arf}^{-/-}*, *BubR1^{H/H}*, and *BubR1^{H/H}/p19^{Arf}^{-/-}* mice. We note that *BubR1^{H/H}* and *BubR1^{H/H}/p19^{Arf}^{-/-}* curves are not statistically different using a log-rank test.

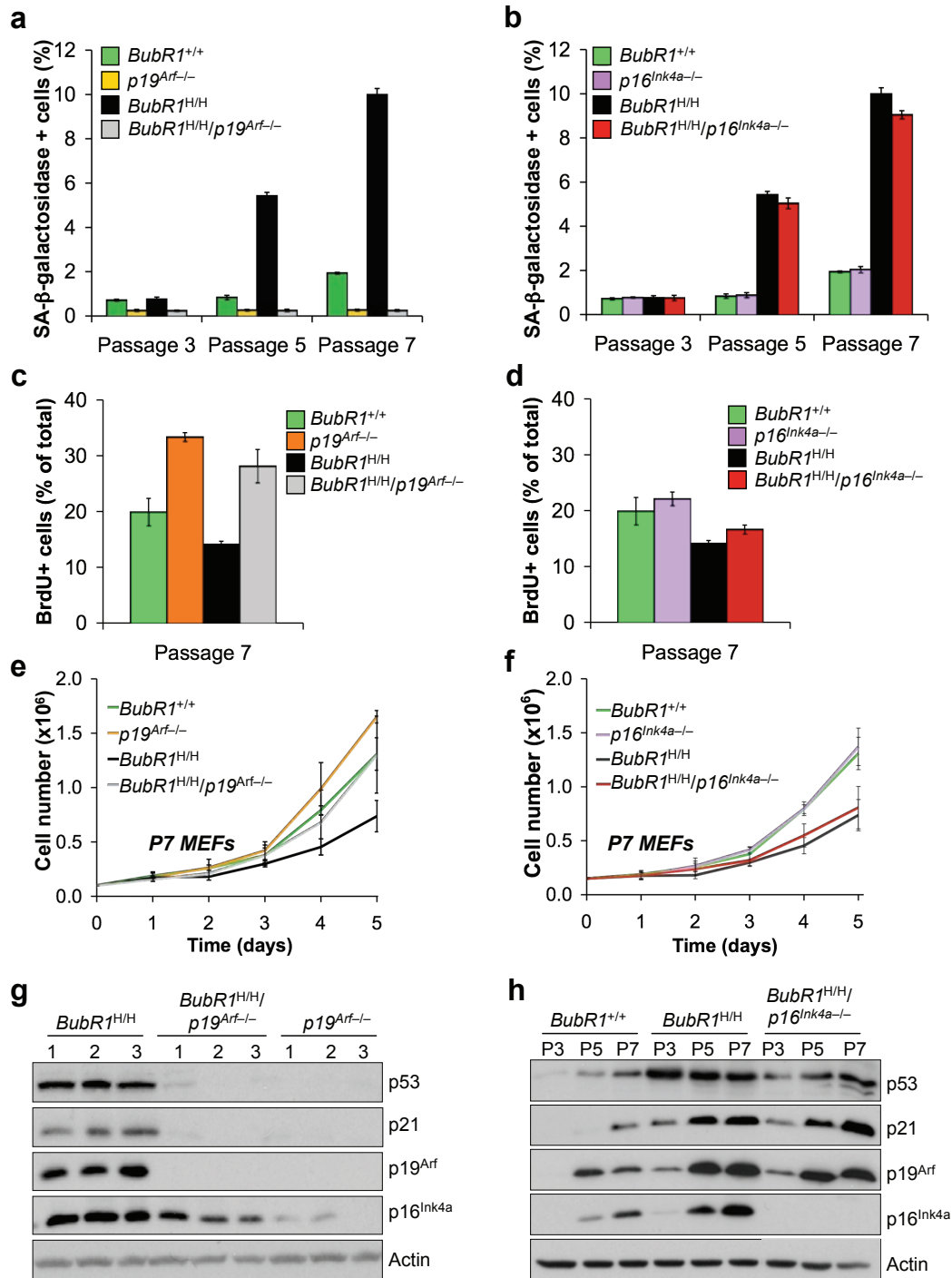


Figure S5 *In vivo* and *in vitro* effects of p16^{Ink4a} and 19^{Arf} ablation on cellular senescence are dissimilar. (a and b) Percentages of SA-beta-galactosidase positive cells in P3, P5 and P7 MEF cultures of the indicated genotypes. For each genotype and passage, three independent MEF lines were scored for SA-beta-galactosidase staining. Error bars are s.d. (c and d) Percentages of cycling cells in P7 MEF cultures of the indicated genotypes as measured by BrdU incorporation. Three independent MEF lines were used for each genotype. Error bars are s.d. (e and f) *In vitro* growth curves of P7 MEF cultures of the indicated genotypes. On day 0, 1.5 x 10⁵ cells were seeded in duplicate and counted for five consecutive days thereafter in

three independent lines of each genotype. Compared to wild-type MEFs, the proliferative capacity of both *BubR1*^{H/H} and *BubR1*^{H/H}/*p16*^{Ink4a-/-} MEFs was greatly reduced but that of *BubR1*^{H/H}/*p19*^{Arf-/-} was not. Lines represent three independent MEF lines per genotype. Error bars are s.d. (g) Western blots of extracts from P7 MEFs of the indicated genotypes probed for p16^{Ink4a}, p19^{Arf}, p53 and p21. Extracts from three independent MEF lines (1-3) were loaded for each genotype. (h) Western blots of extracts from P3, P5, and P7 MEFs of the indicated genotypes were probed for p16^{Ink4a}, p19^{Arf}, p53 and p21. Blots are representative of three independent MEF lines of each genotype. Actin was used as a loading control.

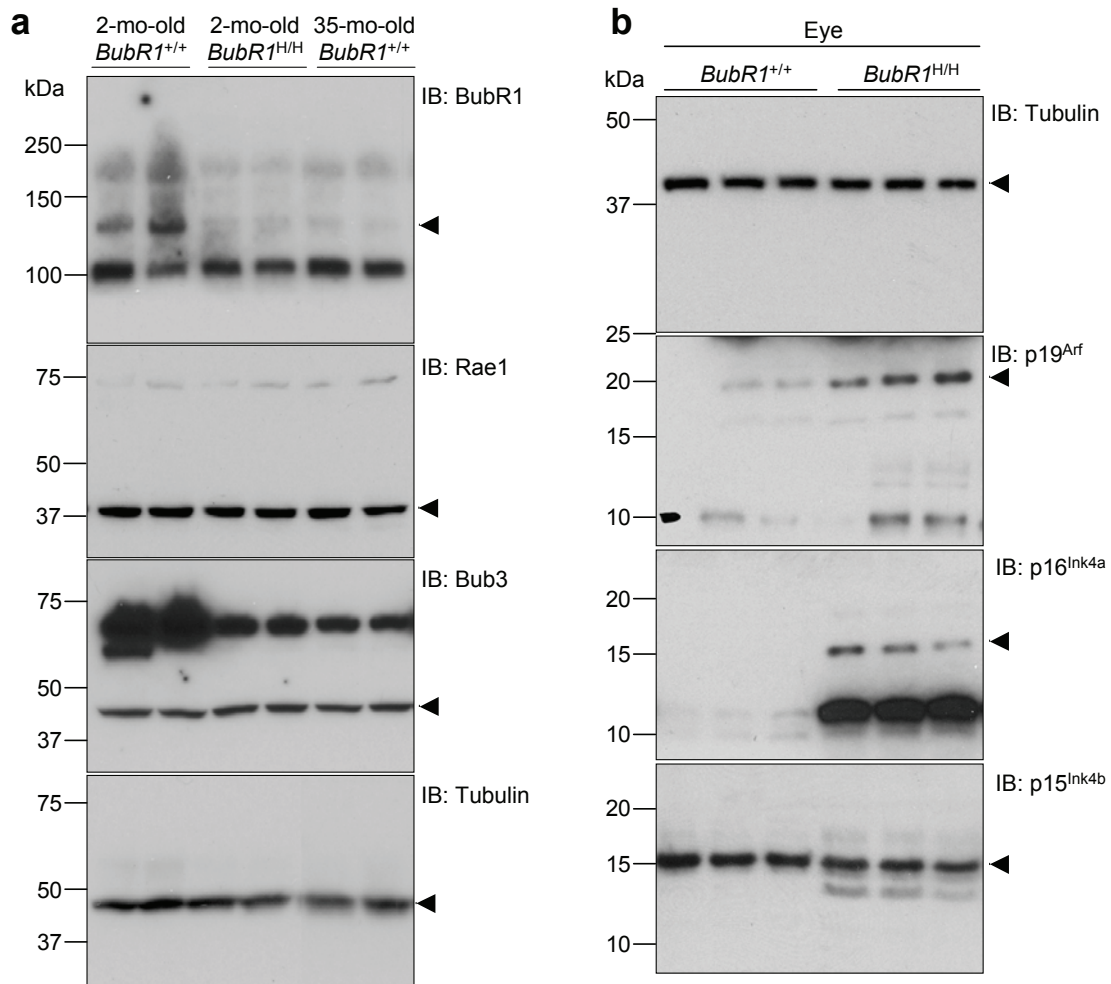


Figure S6 Uncropped images of the western blots shown in: (a) Fig. 2a, (b and c) Fig. 3d and Fig. 5c, (d) Fig. 6f. Blots were cut horizontally into two

portions prior to antibody incubations. Arrowheads indicate specific bands shown in cropped images.

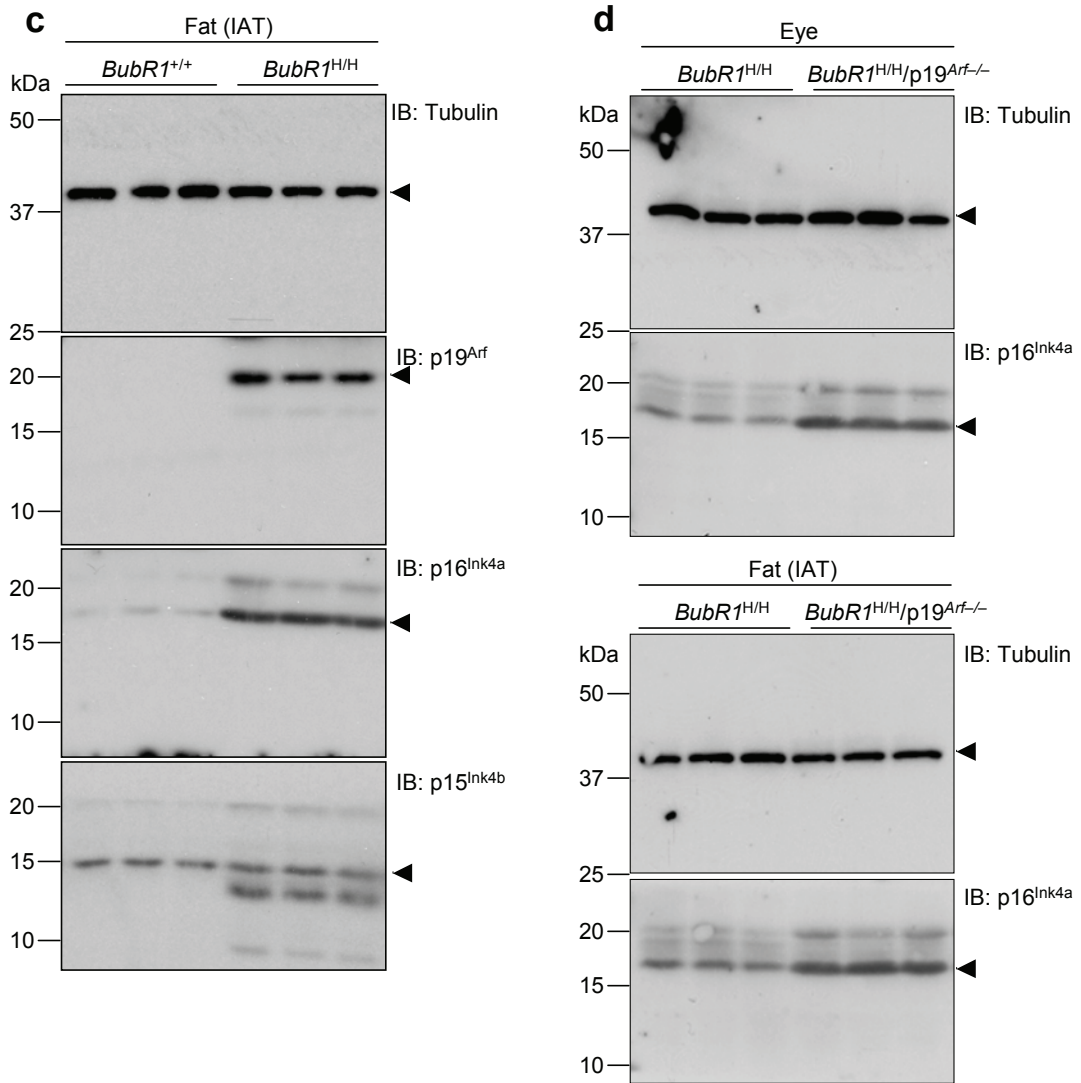


Figure S6 continued

Table S1

Analysis of progeroid phenotypes in *BubR1*^{H/H} mice lacking p16^{Ink4a} or p19^{Arf}

Aging Characteristic	Effect in <i>BubR1</i> ^{H/H} / <i>p16</i> ^{Ink4a-/-} mice compared with <i>BubR1</i> ^{H/H} mice [p value]	Effect in <i>BubR1</i> ^{H/H} / <i>p19</i> ^{Arf-/-} mice compared with <i>BubR1</i> ^{H/H} mice [p value]
Survival	Improved (+) [p = 0.0142]	Unchanged
Lordokyphosis	Improved (+++) [p < 0.0001]	Worsened (++) [p < 0.0001]
Abdominal wall integrity	Improved (+++)	Worsened (++)
Respiratory function	Improved (++) [p < 0.05]	N.D.
Cataract formation	Improved (+) [p < 0.0001]	Worsened (+) [p < 0.0001]
Subdermal adipose	Improved (++) [p = 0.0037]	Worsened (++) [p < 0.0001]
Adipose deposition	Increased (++) [p = 0.003]	Reduced (++) [p = 0.0008]
Anaesthesia tolerance	Improved (+++)	Worsened (+)
Dermal thickness	Unchanged	Unchanged
Dwarfism	Unchanged	Unchanged
Infertility	Unchanged	Unchanged
Arterial wall stiffening	Unchanged	Unchanged

Supplementary Discussion

The only discernible adverse effect of p16^{Ink4a} inactivation in BubR1 hypomorphic mice was an acceleration of lung tumorigenesis. The simplest explanation for this effect would be that p16^{Ink4a} is induced in BubR1 hypomorphic lung tissue as part of a tumor-suppressive mechanism triggering senescence of cells that are at risk for neoplastic transformation. We extensively screened BubR1 hypomorphic lungs for the presence of premalignant lesions, but none were found (data not shown). This precluded us from testing whether p16^{Ink4a} levels are indeed elevated in such lesions. Alternatively, as aneuploidy has been shown to promote tumorigenesis in certain mouse tissues¹, it is conceivable that the numerical chromosome instability resulting from BubR1 insufficiency cooperates with p16^{Ink4a} loss in lung tumorigenesis. Our data demonstrating that p16^{Ink4a} inactivation accelerates lung tumorigenesis in BubR1 hypomorphic mice provides a first example of synergy between a mitotic checkpoint gene defect and a cancer gene mutation. Our observation that BubR1 insufficiency does not cooperate with p19^{Arf} loss in tumorigenesis, suggests that the genetic context or microenvironment in which mitotic checkpoint gene defects promote tumorigenesis is limited.

Reference

1. Weaver, B.A., Silk, A.D., Montagna, C., Verdier-Pinard, P. & Cleveland, D.W. Aneuploidy acts both oncogenically and as a tumor suppressor. *Cancer cell* **11**, 25-36 (2007).